

# Continuous-Time Markov Chain Modeling of Drug-Induced Resistance Continuum

Terry (Taehan) Kim, Joon Kim, Jiyu Beak

December 18, 2025

## Abstract

Drug resistance in cancer emerges through dynamic changes in cell-state composition along a continuum of phenotypic states rather than a single binary switch. In this work, we construct a dose-dependent Continuous-Time Markov Chain (CTMC) model to describe transitions along a resistance axis. Using experimentally measured cell-state compositions across drug doses, we infer dose-dependent transition and death rates and show that the learned rates recapitulate key biological expectations: more resistant states exhibit lower death rates and forward transitions towards resistant phenotypes are favored at higher doses. Our framework provides a quantitative, interpretable view of drug-induced adaptation along a resistance continuum.

## 1 Introduction and Motivation

Analysis of drug resistance remains a major challenge in immunotherapy. Even under tightly controlled experimental conditions, cancer cells can respond very differently to the same drug dose, reflecting underlying heterogeneity and stochasticity in cellular state transitions.

Recent work by Franca et al.[1] demonstrated that resistance does not arise through a single genetic or phenotypic switch. Instead, cancer cells progress along a continuum of phenotypic states, beginning with epithelial and drug-sensitive states ( $CD24^{\text{low}}$   $CD44^{\text{low}}$ ), moving through hybrid EMT-like intermediates, and ultimately reaching highly resistant, stem-like phenotypes ( $CD44^{\text{high}}$ ). These phenotypes can be discretized into five dominant states (S1–S5), where higher drug doses selectively enrich more resistant states (S4–S5).

This progression suggests that drug adaptation can be formulated as a stochastic dynamical process, in which transitions between resistance states and the probability of cell death depend on the applied drug dose. However, the original experimental study does not provide a quantitative framework to infer the specific rates at which these transitions occur or how they vary across drug concentrations.

Our work aims to address this gap by developing a mathematically grounded model capable of inferring dose-dependent transition and death rates along the resistance continuum. Using a continuous-time Markov chain (CTMC) modulated by a biologically plausible Hill dose-response function, we reconstruct the underlying dynamics that give rise to the observed enrichment of resistant states under increasing drug pressure.

## 2 Methodology and Model Setup

### 2.1 Experimental data and state-space definition

We analyze a dataset derived from the Kuramochi cell line, in which cells are exposed to increasing concentrations of a drug. This cell line was selected because the measurements for the data correspond to a relatively homogeneous setup, allowing state transitions to be interpreted as resistance adaptation within a single lineage rather than as mixing between distinct cell types.

For each dose, the experiment reports counts of cells assigned to phenotypic states along the resistance continuum described in [1]. In our analysis, we use six live states: S0\_Control, representing the baseline control population at dose C (no drug); S1 and S2, corresponding to epithelial CD24<sup>low</sup>/CD44<sup>low</sup> drug-sensitive states; S3 and S4, representing hybrid EMT-intermediate markers associated with partial resistance; and S5, a CD44<sup>high</sup> stem-like state associated with high resistance. We additionally introduce a seventh absorbing state SD to represent drug-induced cell death or experimental dropout, which is not directly observed in the proportions but is inferred through the learned CTMC dynamics.

Table 1 summarizes the biological interpretation of each state along the resistance axis.

Table 1: Summary of states along the resistance continuum.

State	Biological meaning	Expected sensitivity
S0	Control (baseline)	Highest sensitivity
S1–S2	Epithelial CD24 <sup>low</sup> /CD44 <sup>low</sup>	Sensitive
S3–S4	Hybrid EMT–intermediate markers	Moderately resistant
S5	Stem-like CD44 <sup>high</sup>	Highly resistant
SD	Death (absorbing)	N/A (inferred)

Each nominal dose label (e.g. “C”, “T1”, “T2.5”) is mapped to a numeric dose value  $D \geq 0$ , with “C” mapped to  $D = 0$  and “Tx” mapped to  $D = x$ . Due to the qualitative nature of the original experiment, it is more informative to observe the proportion of each cell state at each dose. For each dose  $D$ , the raw counts  $c_i(D)$  for  $i \in \{S0, S1, \dots, S5\}$  are converted to proportions

$$p_i(D) = \frac{c_i(D)}{\sum_{j \in \{S0, \dots, S5\}} c_j(D)}. \quad (1)$$

This yields an observed composition vector over live states,

$$\mathbf{P}_{\text{obs}}(D) = (p_{S0}(D), p_{S1}(D), \dots, p_{S5}(D)) \in \mathbb{R}^6. \quad (2)$$

We treat  $\mathbf{P}_{\text{obs}}(D=0) = \{1, 0, \dots, 0, 0\}$  as the initial distribution for the CTMC over the augmented state space  $\{S0, S1, \dots, S5, SD\}$ .

To encode biological constraints on how cells move along the resistance axis, we impose a sparse generator structure for the CTMC. Forward and backward transitions occur only between adjacent states on the continuum, and each live state includes a possible transition to the absorbing death state SD. All other off-diagonal transitions are set to zero. The resulting pattern of allowed

transition rates is summarized below:

$$Q(D) = \begin{bmatrix} S0 & S1 & S2 & S3 & S4 & S5 & SD \\ S0 & \Delta_{00} & \lambda_{01}(D) & \circ & \circ & \circ & \lambda_{0D}(D) \\ S1 & \lambda_{10} & \Delta_{11} & \lambda_{12}(D) & \circ & \circ & \lambda_{1D}(D) \\ S2 & \circ & \lambda_{21}(D) & \Delta_{22} & \lambda_{23}(D) & \circ & \lambda_{2D}(D) \\ S3 & \circ & \circ & \lambda_{32}(D) & \Delta_{33} & \lambda_{34}(D) & \circ & \lambda_{3D}(D) \\ S4 & \circ & \circ & \circ & \lambda_{43}(D) & \Delta_{44} & \lambda_{45}(D) & \lambda_{4D}(D) \\ S5 & \circ & \circ & \circ & \circ & \lambda_{54}(D) & \Delta_{55} & \lambda_{5D}(D) \\ SD & \circ \end{bmatrix} \quad (3)$$

Here,  $\lambda_{ij}(D)$  denotes the dose-modulated rate from state  $i$  to  $j$ ,  $\Delta$  indicates diagonal entries (set to enforce row sums of zero), and  $\circ$  indicates fixed zeros corresponding to biologically disallowed transitions. This structure encodes the assumption that resistance increases through incremental phenotypic steps (e.g.  $S2 \rightarrow S3$ ), that reversion(e.g.  $S4 \rightarrow S3$ ) may have a different rate from its forward counterpart, and that cells may die from any live state. Further descriptions of dose dependence and model training can be found in supplementary information A.2-A.4.

### 3 Results

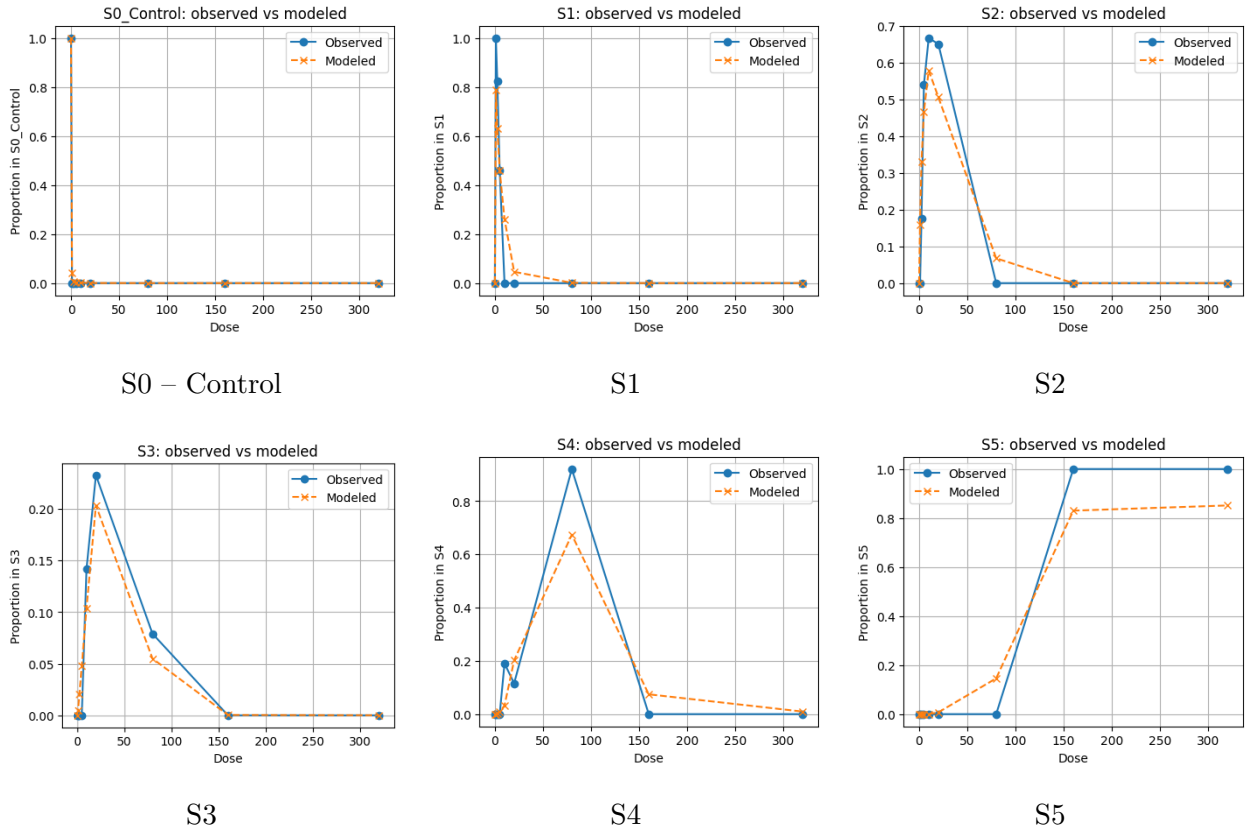


Figure 1: Observed vs CTMC-modeled state trajectories across doses for all six states (S0–S5).

### 3.1 Modeled state compositions fit the observed data

Figure 1 compares the observed ( $\mathbf{P}_{\text{obs}}$ ) and modeled ( $\mathbf{P}_{\text{model}}$ ) state proportions across doses for each live state S0–S5. The model-inferred state compositions follow the observed data. The difference in the peaks can be attributed to the accumulation of death states. A stacked bar plot view (Fig. 2) further illustrate that the overall live-state composition shifts from predominantly S0 at  $D = 0$  to a mixture with significant S4–S5 contributions at higher doses. One interesting observation is that these proportion shifts are more “smooth” compared to the observed data which has more abrupt changes in its composition.

### 3.2 Learned death rates and states along the resistance axis

Table 2: Off-diagonal CTMC rate matrix  $\lambda_{ij}(D)$  at dose  $D = 160$ . Rows denote source states and columns denote target states. The last column corresponds to drug-induced death (SD).

	S0	S1	S2	S3	S4	S5	SD
S0	-	1256.16638	0.00000	0.00000	0.00000	0.00000	4.31657
S1	9.20193	-	97.71190	0.00000	0.00000	0.00000	1.68320
S2	0.00000	1.22725	-	25.94206	0.00000	0.00000	0.76601
S3	0.00000	0.00000	0.94402	-	56.18442	0.00000	0.36723
S4	0.00000	0.00000	0.00000	0.22844	-	3.27783	0.05893
S5	0.00000	0.00000	0.00000	0.00000	0.02778	-	0.04957
SD	0.00000	0.00000	0.00000	0.00000	0.00000	0.00000	0.00000

One key biological expectation is that more resistant states should exhibit lower drug-induced death rates. To evaluate whether the learned CTMC generator  $Q(D)$  satisfies this principle, we extract the off-diagonal entries corresponding to death transitions  $S0 \rightarrow SD, \dots, S5 \rightarrow SD$  and examine how these rates vary with both state identity and dose.

Across all doses  $D$ , the learned death rates follow a strict monotonic ordering:

$$\lambda_{S0,SD}(D) > \lambda_{S1,SD}(D) > \dots > \lambda_{S5,SD}(D), \quad (4)$$

indicating that less resistant states undergo higher instantaneous drug-induced death than in more resistant states. The rates as shown in Table 2 confirms this pattern numerically. Importantly, this monotonic relationship was not enforced as a constraint during training. Instead, it emerged naturally during the optimization function defined, indicating that the inferred structure of  $Q(D)$  captures biologically meaningful differences in drug sensitivity.

### 3.3 Forward and backward transitions along the continuum

We study the forward rates  $\lambda_{S_i,S_{i+1}}(D)$  and backward rates  $\lambda_{S_{i+1},S_i}(D)$  as functions of dose (Fig. 3, 4). Specifically, we observe that forward transitions generally increase with dose, while backward transitions tend to be smaller and less dose-sensitive. This aligns with our hypothesis that drug exposure biases the dynamics towards more resistant phenotypes, while making reversion to sensitive states less likely.

Beyond this overall trend, the inferred transition rates also reveal substantial heterogeneity among individual forward transitions. In particular, the  $S0 \rightarrow S1$  transition exhibits the highest rate, suggesting that this step represents the least constrained shift along the continuum. This

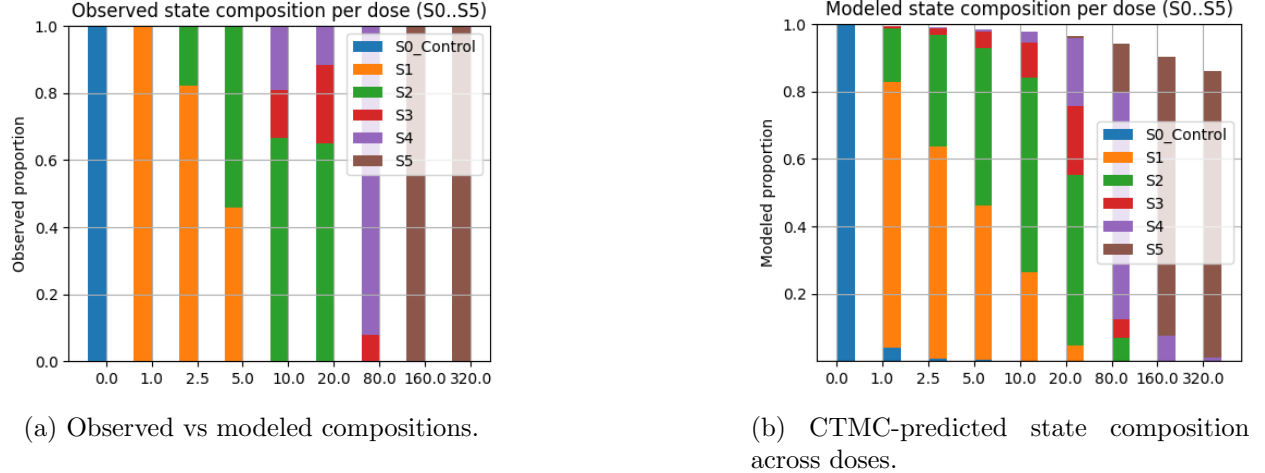


Figure 2: Comparison between observed data and CTMC-modeled state compositions across doses.

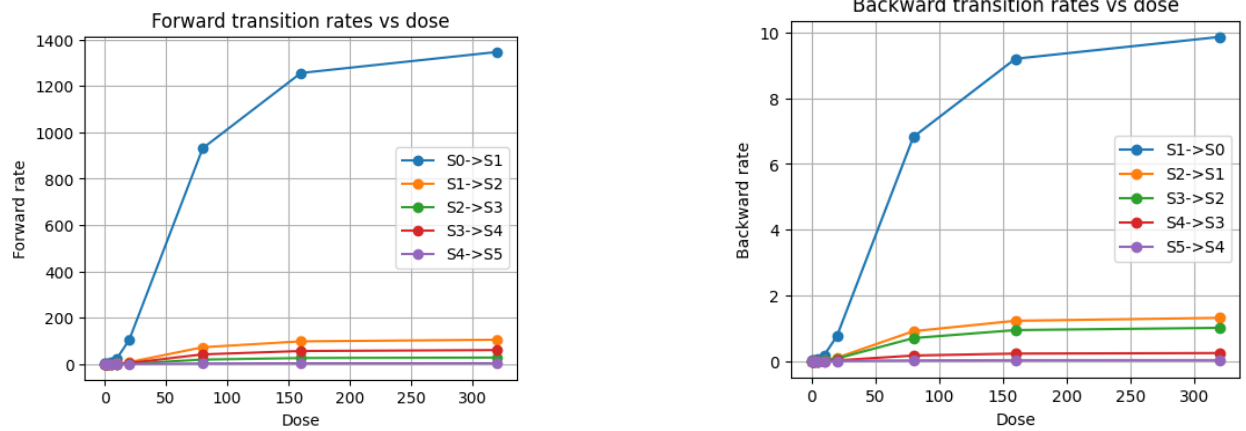


Figure 3: Forward transition rates.

Figure 4: Reverse transition rates.

is consistent with the fact that both states retain predominantly epithelial characteristics and therefore require minimal transcriptional reprogramming.

In contrast, the  $S2 \rightarrow S3$  transition emerges as a relative bottleneck, with transition rates that are consistently lower than those of the subsequent  $S3 \rightarrow S4$  step. This subtle but reproducible difference indicates that progression into State 3 poses a greater barrier than later transitions. From a biological perspective, this observation aligns with the initiation of a hybrid EMT-like program at State 3, which involves substantial changes in cytoskeletal organization, extracellular matrix interactions, and transcriptional regulation, as reflected by the activation of EMT-associated genes such as SOX4 and VIM.

Once cells enter this EMT-like regime, subsequent transitions toward more dedifferentiated states appear less constrained, consistent with the higher  $S3 \rightarrow S4$  transition rates observed in the model. Taken together, these results suggest that resistance evolution is shaped not only by a general forward bias under drug pressure, but also by uneven transition barriers, with the  $S2 \rightarrow S3$  step representing a key rate-limiting transition along the resistance continuum.

## 4 Discussion

Our Hill-modulated CTMC model provides a compact and interpretable model of drug-induced adaptation along a resistance continuum. Several aspects of the learned dynamics align with biological intuition and prior experimental observations:

- **Monotonic death rates along the resistance axis:** More sensitive states experience higher drug-induced death rates than more resistant states at all doses.
- **Dose-biased forward transitions:** Higher doses favor transitions towards more resistant phenotypes, consistent with EMT activation and stem-like reprogramming under drug pressure (as suggested in the original literature).
- **Reconstruction of composition trajectories:** The model successfully captures the shift from predominantly sensitive states at low dose to enriched resistant states at high dose.

From a modeling perspective, the combination of 1) a biologically structured state space of S0–S5 + SD and 2) a sparse CTMC generator matching the resistance transition offers interpretability while capturing key biological insights suggested in the literature.

Beyond faithfully reproducing known resistance trends, this framework also suggests how quantitative modeling of transition dynamics may inform broader biological and therapeutic questions. Although our analysis focuses on olaparib-induced resistance, the inferred transition structure is unlikely to be specific to PARP inhibition alone. Similar non-genetic, EMT-associated adaptation trajectories have been reported for other targeted therapies, including EGFR and BRAF inhibitors, suggesting that the proposed CTMC framework may generalize to a broader class of drugs that reshape cell-state landscapes through phenotypic plasticity.

In addition, the dose-dependent transition dynamics learned by the model highlight regions of the resistance continuum where highly resistant states rapidly expand. Such “danger zones” point to the possibility of using predicted state compositions to identify dosing regimes that inadvertently accelerate resistance, and conversely, to explore strategies that maintain tumor control while delaying the enrichment of deeply resistant phenotypes.

Finally, the modular structure of the model naturally lends itself to future extensions. Incorporating explicit time-course measurements would allow direct inference of transition kinetics, while extending the state space to include multiple drugs could enable the study of drug sequencing or combination strategies. Moreover, modeling a mixture of multiple transition matrices for separate “clusters” could be a compelling choice if one assumes that different cell lineages have varying underlying transition rates.

In this sense, the CTMC framework provides a flexible foundation for integrating biological insight with predictive modeling of resistance evolution. Although we demonstrate this framework using a tumor cell system, the underlying principles of non-genetic plasticity and stochastic state transitions are not cancer-specific. Similar continuous state dynamics govern many immune cell populations, such as T cell exhaustion, macrophage polarization, and dendritic cell maturation, suggesting that the proposed CTMC framework is directly applicable to various problems studied in single-cell immunology.

Our framework provides a tractable and interpretable model for connecting phenotypic state distributions to underlying dynamical mechanisms, and can serve as a template for modeling other systems where stochastic state transitions and dose-dependent selective pressures shape population-level responses. However, it comes with a limitation that it is based on very limited data, and we therefore suggest that a more continuous and controlled dataset be collected if similar modeling is intended to be used.

## 5 Contributions

Terry Kim, Joon Kim, and Jiyu Beak formulated the question and direction together. Terry and Joon implemented the algorithm, code, and figures. Jiyu Baek helped aligning towards biologically relevant direction.

## References

- [1] Gustavo S. França, Maayan Baron, Benjamin R. King, Jozef P. Bossowski, Alicia Bjornberg, Maayan Pour, Anjali Rao, Ayushi S. Patel, Selim Misirlioglu, Dalia Barkley, Kwan Ho Tang, Igor Dolgalev, Deborah A. Liberman, Gal Avital, Felicia Kuperwaser, Marta Chiodin, Douglas A. Levine, Thales Papagiannakopoulos, Andriy Marusyk, Timothée Lionnet, and Itai Yanai. Cellular adaptation to cancer therapy along a resistance continuum. *Nature*, 631(8022):876–883, July 2024. Publisher: Nature Publishing Group.

## A Supplementary Information

### Data Availability

scRNA-Seq: Kuramochi data discussed in this manuscript have been originally deposited in the NCBI Gene Expression Omnibus (GEO) and are accessible through accession number **GSE247691**. The raw data can be found at:

- Data: <https://www.ncbi.nlm.nih.gov/geo/query/acc.cgi?acc=GSE247691>

### Code Availability

The code to reproduce the results in this manuscript is available at [https://github.com/YosefLab/Thymus\\_CITE-seq](https://github.com/YosefLab/Thymus_CITE-seq) and has been deposited at [10.5281/zenodo.8102050](https://zenodo.10.5281/zenodo.8102050) (ref. 73).

#### A.1 The generator matrix

We first rigorously define the generator matrix. The evolution of cell states as a CTMC on the state space

$$\mathcal{S} = \{S0, S1, S2, S3, S4, S5, SD\}, \quad (5)$$

with a dose-dependent generator (rate) matrix  $Q(D) \in \mathbb{R}^{7 \times 7}$ :

$$Q(D) = (q_{ij}(D))_{i,j \in \mathcal{S}}. \quad (6)$$

The generator satisfies the standard CTMC constraints:

$$q_{ij}(D) \geq 0, \quad i \neq j, \quad (7)$$

$$q_{ii}(D) = - \sum_{j \neq i} q_{ij}(D), \quad \text{so that} \quad \sum_j q_{ij}(D) = 0. \quad (8)$$

The transitions are also defined as below:

- **Nearest-neighbor transitions along the resistance axis:**

$$\lambda_{ij} \quad \text{for} \quad S0 \leftrightarrow S1, \quad S1 \leftrightarrow S2, \quad S2 \leftrightarrow S3, \quad S3 \leftrightarrow S4, \quad S4 \leftrightarrow S5. \quad (9)$$

- **Death transitions from each live state:**

$$\lambda_{iD} \quad \text{for} \quad S0 \rightarrow SD, \dots, S5 \rightarrow SD. \quad (10)$$

- **Absorbing death state:**

$$q_{SD,j}(D) = 0 \quad \text{for all } j \in \mathcal{S}. \quad (11)$$

Each rows sum up to 0, noting that each rate transition is preserved. All other off-diagonal entries are fixed to zero. This encodes the biological assumption that cells traverse the resistance continuum in relatively small phenotypic steps and can die from any live state.

## A.2 Dose modulation via a Hill function

For each allowed transition  $i \rightarrow j$ , we define a dose-dependent rate

$$\lambda_{ij}(D) = \theta_{ij} f(D), \quad (12)$$

where  $\theta_{ij} > 0$  is a baseline rate parameter and  $f(D)$  is a shared Hill-type dose-modulation function,

$$f(D) = 1 + \alpha \frac{D^n}{K^n + D^n}. \quad (13)$$

Here,  $K > 0$  is an effective EC<sub>50</sub>,  $n > 0$  is the Hill coefficient controlling the steepness, and  $\alpha > 0$  controls the maximum fold-change relative to baseline (i.e.  $f(D) \rightarrow 1 + \alpha$  as  $D \rightarrow \infty$ ).

In our implementation, the parameters  $(\theta_{ij})$ ,  $K$ ,  $n$ , and  $\alpha$  are represented in log-space and learned using gradient-based optimization in PyTorch.

Given  $\lambda_{ij}(D)$  for allowed transitions, the off-diagonal entries of  $Q(D)$  are set as

$$q_{ij}(D) = \lambda_{ij}(D), \quad i \neq j, \quad (14)$$

and the diagonal entries are adjusted to ensure each row sums to zero:

$$q_{ii}(D) = - \sum_{j \neq i} q_{ij}(D). \quad (15)$$

## A.3 Time evolution and transition kernel

For a fixed dose  $D$ , the transition kernel over a unit time interval  $\Delta t = 1$  is given by the matrix exponential

$$P(D) = \exp(Q(D) \Delta t). \quad (16)$$

If  $\boldsymbol{\pi}(t)$  denotes the row vector distribution over states at time  $t$ , then

$$\boldsymbol{\pi}(t + \Delta t) = \boldsymbol{\pi}(t) P(D). \quad (17)$$

In the dose trajectory, we assume that between two measured doses  $D_k$  and  $D_{k+1}$ , the cell population evolves under the generator  $Q(D_k)$  over an effective time interval  $\Delta t = 1$ , expressed in arbitrary units.<sup>1</sup> This corresponds to treating each measured dose condition as a discrete step along an otherwise continuous-time process. Let  $\boldsymbol{\pi}(t)$  denote the row vector of state probabilities over the augmented state space  $(S0, S1, \dots, S5, SD)$ . The initial distribution at the control condition is constructed as

$$\boldsymbol{\pi}(D_1) = [\mathbf{P}_{\text{obs}}(D_1) \ 0], \quad (18)$$

where the last coordinate, corresponding to the absorbing death state SD, is initialized to zero. For each subsequent dose, we propagate the distribution forward using the transition kernel

$$P(D_k) = \exp(Q(D_k) \Delta t), \quad (19)$$

so that

$$\boldsymbol{\pi}(D_{k+1}) = \boldsymbol{\pi}(D_k) P(D_k). \quad (20)$$

At each step, the live-state portion of  $\boldsymbol{\pi}(D_k)$  is extracted as the modeled composition

$$\mathbf{P}_{\text{model}}(D_k) \in \mathbb{R}^6, \quad (21)$$

allowing direct comparison with the experimentally observed proportions.

---

<sup>1</sup>The choice of  $\Delta t$  is a design choice that is not entirely rigorous; it assumes that by that time, the interaction between the dose and cells has reached a steady state. For other datasets, a different value might be more adept.

#### A.4 Loss functions (Objective Function) and parameter estimation

Model parameters are estimated by minimizing the discrepancy between  $\mathbf{P}_{\text{model}}(D_k)$  and the experimentally observed compositions  $\mathbf{P}_{\text{obs}}(D_k)$  across all doses. Let  $K$  denote the number of distinct dose conditions. We consider two loss formulations that emphasize different aspects of the fit.

**L2 loss.** The first objective penalizes squared deviations between modeled and observed compositions,

$$\mathcal{L}_{\text{L2}} = \frac{1}{K} \sum_{k=1}^K \|\mathbf{P}_{\text{model}}(D_k) - \mathbf{P}_{\text{obs}}(D_k)\|_2^2, \quad (22)$$

which directly measures how close the predicted proportions are in magnitude to their empirical counterparts. This is defined following the standard choice for optimization tasks.